RSC Advances

PAPER

View Article Online
View Journal | View Issue

Cite this: *RSC Adv.*, 2024, **14**, 4025

A solid-state electrolyte for electrochemical lithium–sulfur cells†

Yi-Chen Huang,[a] Bo-Xian Ye[a] and Sheng-Heng Chung *[ab]

Received 31st August 2023
Accepted 10th January 2024

DOI: 10.1039/d3ra05937e

rsc.li/rsc-advances

Post-lithium-ion batteries are designed to achieve high energy density and high safety by modifying their active material and cell configuration. In terms of the active material, lithium–sulfur batteries have the highest charge-storage capacity and high active-material utilization because of the use of a conversion-type sulfur cathode, which involves conversion between solid-state sulfur, liquid-state polysulfides, and solid-state sulfides. In terms of the configuration, solid-state batteries ensure high safety by using a solid-state electrolyte in between the two electrodes. Herein, we use a lithium lanthanum titanate (LLTO) solid-state electrolyte in the lithium–sulfur cell with a polysulfide catholyte electrode. The LLTO, which replaces the conventional liquid electrolyte, is a solid-state electrolyte that offers smooth lithium-ion diffusion and prevents the loss of polysulfides, while the highly active polysulfide electrode, which replaces the solid-state sulfur cathode, improves the reaction kinetics and the active-material utilization. The material and electrochemical analyses confirm the stabilized electrodes exhibit long-lasting lithium stripping/plating stability and limited polysulfide diffusion. Moreover, the morphologically and electrochemically smooth interface between the solid-state electrolyte and catholyte enables fast charge transfer in the cell, which demonstrates a high charge-storage capacity of 1429 mA h g^{-1}, high rate performance, and high electrochemical efficiency.

Introduction

With the rapid development of the functions and sizes of electrical devices since 1991, the demand for energy-storage systems has been boosted by the commercialization of lithium-ion batteries. The high energy density of these batteries results from the lithium cobalt oxide cathode with a theoretical charge-storage capacity of 274 mA h g^{-1} and ~50% electrochemical utilization, resulting in a high specific capacity of 140 mA h g^{-1}. After a 30 year development, the material combination and component design of lithium-ion technology have reached maturity, and the progress of the lithium-ion battery concerning its theoretical performance has almost reached a standstill, while the price keeps increasing.[1–4] Therefore, post-lithium-ion battery systems now attract widespread attention. In terms of cell electrochemistry, conversion-type electrochemical lithium–sulfur batteries, which have a high charge-storage capacity of 1675 mA h g^{-1} contributed by sulfur to offer a high theoretical energy density of 2600 W h kg^{-1}, nontoxicity, and low material cost (USD 100 per ton for sulfur), are regarded as the most promising candidates for next-generation energy-storage devices.[3–7] In terms of the cell configuration, solid-state electrolytes, with wide operating voltage windows, excellent chemical stability, and superior safety, are under study for use in advanced rechargeable batteries.[4,8–11] However, as the future mainstays of battery materials and configurations, respectively, lithium–sulfur batteries and solid-state electrolytes face several challenges that will impede commercialization until they are overcome.[10–14]

For the lithium–sulfur battery, the insulating nature of solid-state sulfur (and sulfide at the discharge stage), the generation of liquid-state polysulfides during cycling, and the solid–liquid–solid conversion of the active material together lead to sluggish reaction kinetics, fast loss of active material, and unstable transition between phases, respectively. These materials shortcomings give rise to a common perception of lithium–sulfur cells as being blighted by low electrochemical utilization, efficiency, and stability.[4–6] Additionally, polysulfide is highly soluble in liquid electrolytes, making it difficult to restrain its diffusion to the anodic area. Once the polysulfide diffuses to the anodic area and reacts with the lithium anode, it generates insulating lithium sulfide and deposits on the surface of the lithium electrode, leading to irreversible active-material loss and corrosion of the lithium anode.[5–7] This problem has been intensively addressed using strategies such as the application of porous materials,[3–7,15] modified separators,[4–7,16] or multi-layer electrolytes[3–7,17] as sulfur hosts or polysulfide barriers to

[a]*Department of Materials Science and Engineering, National Cheng Kung University, No. 1, University Road, Tainan City, 70101, Taiwan. E-mail: SHChung@gs.ncku.edu.tw*

[b]*Hierarchical Green-Energy Materials Research Center, National Cheng Kung University, No. 1, University Road, Tainan City, 70101, Taiwan*

† Electronic supplementary information (ESI) available: XRD, SEM, EDS analysis. See DOI: https://doi.org/10.1039/d3ra05937e

mitigate polysulfide diffusion. The stabilized polysulfides in the cathode region of the cell would contribute their high reaction activity to the conversion reaction of cathode, which results in the high active-material utilization and reaction kinetics. Thus, polysulfides have been adopted as the novel catholyte system for high-performance lithium–sulfur cell.[16–19] However, these strategies have demonstrated limited effectiveness. It is necessary to expedite the development of innovative and reliable methods for the high-energy-density application of the lithium–sulfur battery.[4,5,12–14] In sum, despite its many merits, the development of the lithium–sulfur battery is still hindered by the insulating nature of solid-state sulfur/sulfide and the generation of liquid-state polysulfides during cycling.[5–7]

For the solid-state electrolytes, the poor lithium-ion conductivity of the material itself as compared to that of liquid electrolyte and the high interface impedance when combined with a solid electrode to form a solid/solid interface are the major challenges.[4,12–14] Among the solid-state electrolytes studied to date, the solid-state oxide electrolyte has a higher in-cell stability than the solid-state polymer electrolyte and a higher in-atmosphere stability than the solid-state sulfide electrolyte.[11–14] Specifically, among solid-state oxide electrolytes, lithium lanthanum titanate (LLTO) has the highest lithium-ion conductivity (1×10^{-3} S cm^{-1}) and high chemical stability; thus, it has attracted intense research interest in the past decade.[14,20–22] However, the bulk of research into LLTO has been limited to lithium-ion battery systems and few lithium–sulfur battery systems have been reported. Moreover, comprehensive electrochemical analyses and long-term cycling performance tests are rarely reported.[4,8–14,20–22] Thus, despite the potential of solid-state electrolytes to alleviate the risk of explosion during cycling and promote the application of derived solid-state batteries with outstanding safety, the high interface resistance between cathode and electrolyte and limited understanding of solid-state electrolytes in cells greatly impede charge transfer and the coordination of electrolyte and electrode. These further slow the component integration of solid batteries as well as their interface analysis and device optimization.[4,22–24]

In this research, we integrate an electrochemical lithium–sulfur cell with a solid-state electrolyte to demonstrate the possibility of a lithium–polysulfide cell with a LLTO solid-state electrolyte. In this cell configuration, the polysulfide catholyte offers high reactivity and generates a smooth liquid/solid interface between the cathode and electrolyte, which result in a high electrochemical utilization of sulfur above 85%. Meanwhile, the LLTO electrolyte blocks the fast polysulfide diffusion, enables rapid lithium-ion transfer, and stabilizes the lithium anode, which ensures the electrochemical and cycle stabilities of the resulting cell. The cell, therefore, demonstrates long-lasting lithium stripping/plating stability, a high charge-storage capacity of 1429 mA h g^{-1}, and a good rate performance of C/50 – C/3 rates.

Experimental

Material preparation and analysis

The lithium lanthanum titanate (LLTO) solid-state electrolyte was prepared directly using commercial LLTO ceramic powder (NEI Corporation). Specifically, 0.3 g LLTO powder was pressed into a mold with a diameter of 12 mm under a force of 4 metric tons for 1 minute. The pressed green sample was cold isostatically pressed and sintered at 1200 °C for 12 hours in a high-temperature furnace (CTF 12/75/700, Carbolite-Gero) with a ramp rate of 5 °C min^{-1} from room temperature (25 °C) to 1000 °C and 2.5 °C min^{-1} from 1000 °C to 1200 °C. The as-prepared sintered LLTO pellet had a thickness and a diameter of 800–900 μm and 10 mm, respectively. The LLTO pellet was subsequently polished to a thickness of 500 μm to remove possible surface impurities and decomposition products. The resulting LLTO solid-state electrolyte was dried in a vacuum oven and stored in a vacuum chamber. The relative density and crystalline structure of the LLTO pellet were investigated using a gas pycnometer (Ultrapyc 5000 Micro, Anton Paar) and an X-ray diffraction (XRD) spectrometer (D8 Discover with GADDS, Bruker AXS GmbH). The morphology and elemental distribution were analyzed using a field emission scanning electron microscope (SEM, SU8000, Hitachi) and an energy-dispersive X-ray spectrometer (EDS, XFlash Detector 5010, Bruker). The surface chemical analysis was analyzed using a X-ray photoelectron spectrometer (XPS, PHI 5000 VersaProbe, Ulvac-phi) and the data were fitted using CasaXPS software after subtracting the Shirley-type background. The cross-sectional surface investigation of the cycled LLTO solid-state electrolyte was performed using a secondary ion mass spectrometer (SIMS, IMS-7f, Cameca), providing evidence on the precise chemical composition distribution from the top surface to the cathode-facing side of the LLTO solid-state electrolyte.

Electrochemical characteristics and analysis

The electrochemical characteristics of the LLTO solid-state electrolyte were measured using a lithium/lithium symmetric cell and a lithium–polysulfide cell. The lithium electrode (Sigma-Aldrich) was polished and rinsed using a blank electrolyte to remove the surface oxidation products and generate a passivation layer on the lithium electrode to ensure good experimental control.[25,26] The lithium/lithium symmetric cell was set in an EL-cell for electrochemical impedance spectroscopy (EIS) analysis and lithium-ion conductivity measurement using an electrochemical workstation (SP-150, Biologic) at temperatures of 25, 30, 40, 50, 60, and 70 °C and frequencies from 1 MHz to 0.1 mHz. A lithium–polysulfide cell was subsequently prepared with polysulfide catholyte as the starting active material. The polysulfide catholyte was prepared by dissolving sulfur and lithium sulfide (Li_2S) at a stoichiometry of 1 : 5 in a blank electrolyte at 70 °C to form a 0.1 M Li_2S_6 polysulfide catholyte. The polysulfide catholyte was drop-casted onto a carbon substrate to form a polysulfide cathode. The blank electrolyte was prepared by adding 1.85 M $LiN(CF_3SO_2)_2$ salt (Sigma-Aldrich) and 0.5 M $LiNO_3$ co-salt (Sigma-Aldrich) to a mixture of 1,3-dioxolane (Alfa Aesar) and 1,2-dimethoxyethane (Alfa Aesar) at a volumetric ratio of 40 : 55.[22,25] The as-prepared lithium–polysulfide was used for cyclic voltammetry (CV) measurements, using an electrochemical workstation (BCS-800 workstation, Biologic) at a potential sweeping rate of 0.010 mV

s^{-1} in the voltage range of 1.5–3.0 V (*versus* Li/Li^+). Its cyclability, rate performance, and galvanostatic discharge–charge voltage profiles were performed using a battery test system (CT-4008-5 V-10 mA, Neware) in the range of 1.8–2.8 V at the cycling rates of C/50 – C/3. The cycling rate was calculated with 1C set as 1675 mA g^{-1} based on the material's theoretical capacity and the capacity is calculated based on the mass of sulfur in the polysulfide cathode.

Results and discussion

Material and electrochemical characteristics

Fig. 1a and S1† show that the sintered LLTO pellet was stable and retained the same crystalline phase as the parent commercial powder, as evidenced by the XRD pattern with peaks matching those of $Li_{0.33}La_{0.57}TiO_3$ (LLTO). Minor $Li_2La_2Ti_3O_{10}$ impurity phase was found in both LLTO commercial powder and the sintered pellet. $Li_{0.33}La_{0.57}TiO_3$ (LLTO) and $Li_2La_2Ti_3O_{10}$ were thus used for the modelling of Rietveld refinement. Fig. S1a and b† show approximately 20% and 19% of impurity phase in the commercial powder and the sintered pellet, respectively. The observation of the $Li_2La_2Ti_3O_{10}$ phase might result from the inhomogeneous mixing of raw powder in the early stage if the amount of TiO_2 is less.[27] Fig. 1b and c show the morphology and microstructure of the LLTO ceramic inspected from the surface and from the cross section, respectively. The broad-survey and high-magnification scanning electron microscopy (SEM) images show the dense structure and high-density trait of the LLTO ceramic, respectively. The density of the sample was almost 98%, making it suitable for application as a battery electrolyte. Accordingly, we made the lithium–polysulfide cell with the LLTO as the solid-state electrolyte and retrieved the cycled LLTO solid-state electrolyte to observe the anode and cathode sides of cycled the sample. Fig. 1d and e show the anode and cathode side SEM inspection of the cycled LLTO, respectively. Both surfaces of the LLTO were covered by a layer of solid-state electrolyte interlayer, while the formation layers were smooth and had no conglomeration of the cycled by-products.[4–6,8,9] Moreover, the SEM/EDS inspection of the corresponding cycled LLTO solid-state electrolyte facing the lithium electrode and facing the polysulfide electrode showed no and very low elemental sulfur signals, respectively (Fig. S2†). This indicates that the use of solid-state electrolyte well stabilized the polysulfide in the cathode as the catholyte. In addition, Fig. 1f and g show the X-ray photoelectron spectroscopy (XPS) analysis of the cycled LLTO solid-state electrolyte facing the lithium electrode and facing the polysulfide electrode. No lithium sulfides or sulfur were found on the anode side of LLTO (Fig. 1f), while polysulfides and sulfides based compounds were found on the cathode side of LLTO (Fig. 1g). The XPS results further evidence that the LLTO solid-state electrolyte successfully blocks the diffusion of active material from the cathode to the anode.

Fig. 2a and b illustrate the lithium-ion conductivity of the LLTO solid-state electrolyte. To keep good control of the electrochemical analysis with the lithium electrode, we rinsed the commercial lithium ribbon with the blank electrolyte, which

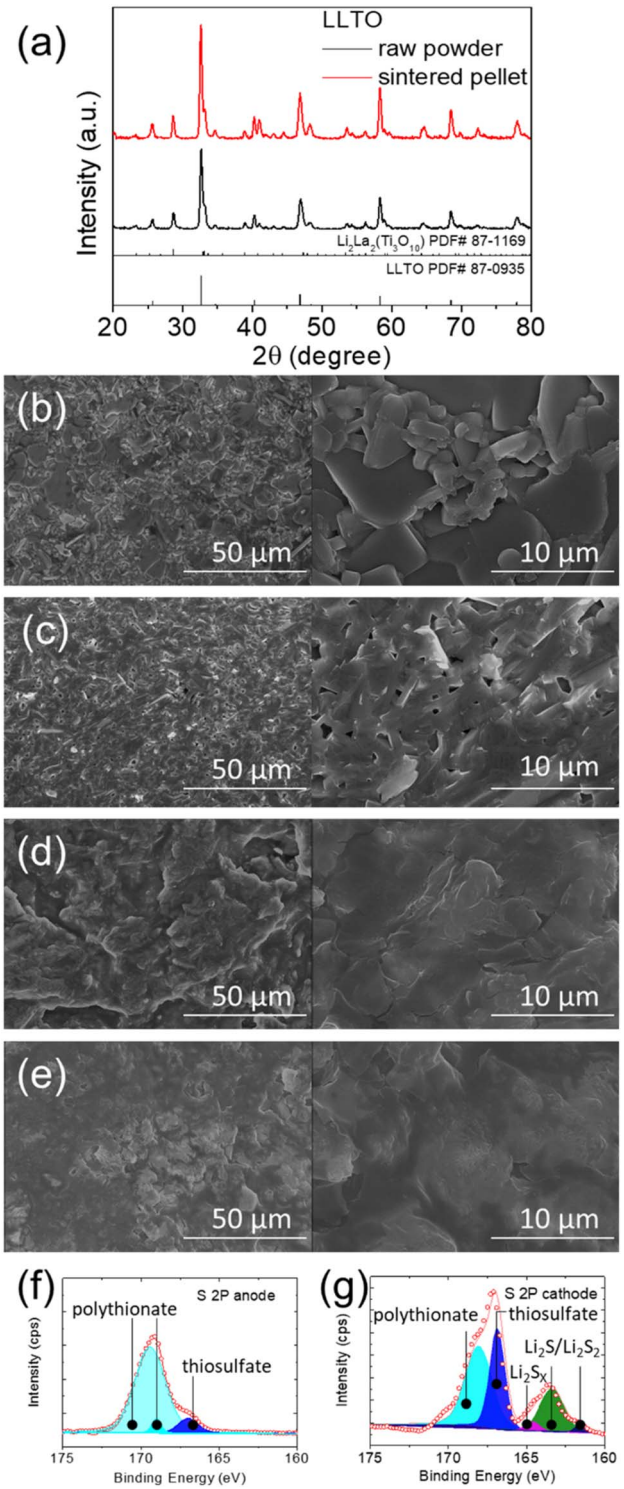

Fig. 1 Material characteristics of lithium lanthanum titanate (LLTO) solid-state electrolyte: (a) X-ray diffraction (XRD) pattern; scanning electron microscopy (SEM) observation with low (left) and high (right) magnifications of (b) surface morphology, (c) cross-sectional microstructure, (d) cycled sample facing the lithium electrode, and (e) cycled sample facing the polysulfide electrode; and X-ray photoelectron spectroscopy (XPS) analysis of cycled sample (f) facing the lithium electrode, and (g) cycled sample facing the polysulfide electrode.

also formed a passivation layer on the clean lithium surface for protection.[25,26,28,29] The electrochemical impedance spectra (EIS) data collected from room temperature (25 °C) to 70 °C were used for Arrhenius-plot analysis, which indicated the high lithium-ion conductivity of 1.2×10^{-3} S cm^{-1} to 3.9×10^{-4} S cm^{-1}. The ionic conductivity of our LLTO was very close to the values of approximately 1.0×10^{-3} S cm^{-1} reported in the literature.[20–22] Fig. 2c shows the lithium stripping/plating analysis using the lithium/lithium symmetric cell equipped with the LLTO solid-state electrolyte. The lithium stripping/plating data indicate the high stability of the cell during the lithium dissolution and deposition processes, which maintained a low overpotential of 0.2 V at 0.05 mA cm^{-2} for a long period of 600 hours and 0.5 V at 0.1 mA cm^{-2} for another long period of 400 hours. These analytical results indicated that the LLTO solid-state electrolyte sustained stable cycling performance under high lithium plating/stripping rates, showed sufficient compatibility with lithium and a strong mechanical structure, and avoided the occurrence of a short-circuit. Moreover, the stable lithium stripping/plating processes revealed the high interfacial stability and sufficient compatibility between LLTO and passivated lithium, as well as the robustness of the LLTO solid-state electrolyte.[20–22,29–31]

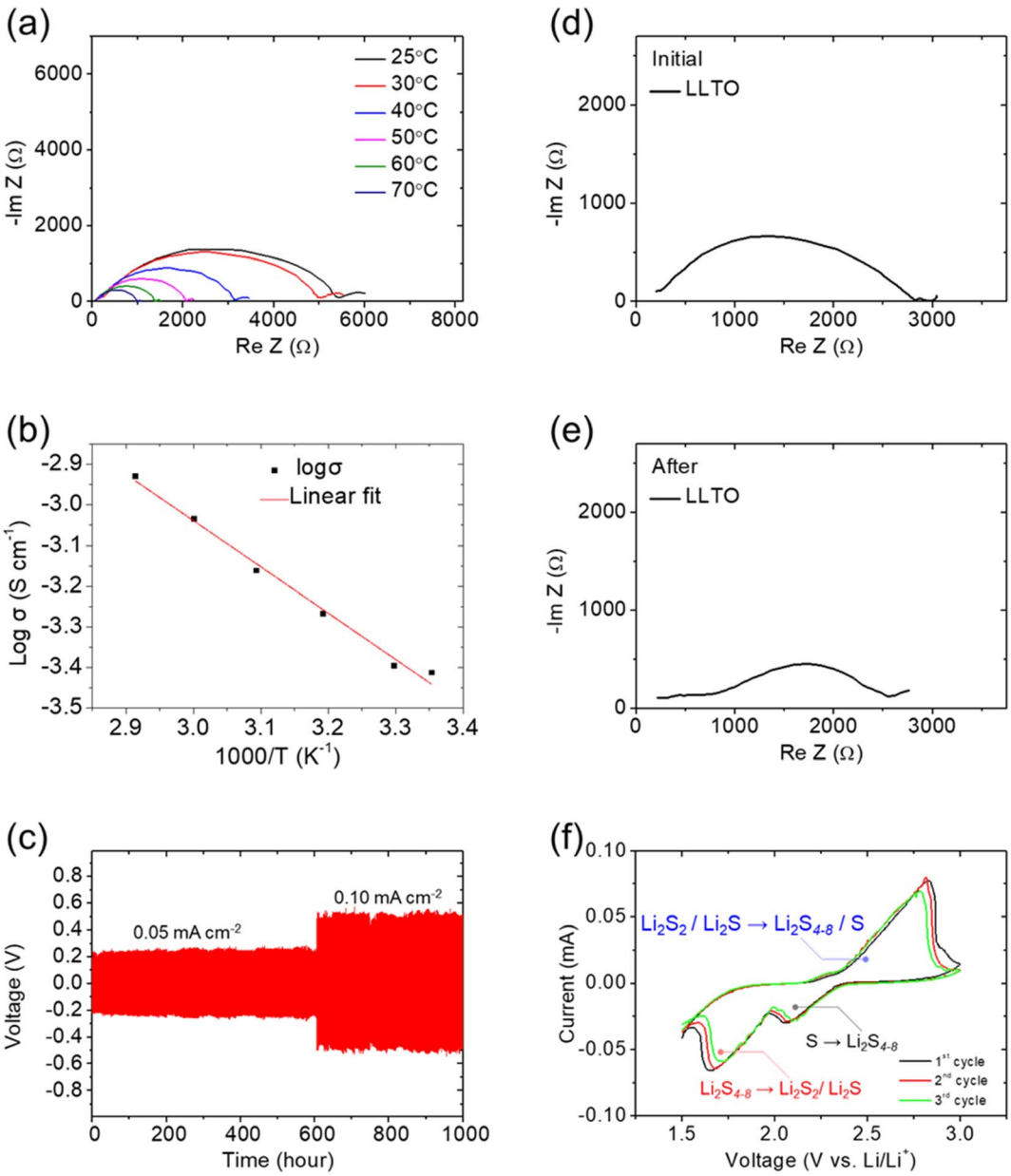

Fig. 2 Electrochemical characteristics of LLTO solid-state electrolyte: (a) electrochemical impedance spectroscopy (EIS) analysis from 25 °C to 70 °C, (b) lithium-ion conductivity, and (c) lithium stripping/platting analysis of lithium/lithium symmetric cell; and EIS analysis (d) before and (e) after cycling, and (f) cyclic voltammetry (CV) profile of lithium–sulfur cell.

The fast and stable lithium-ion transfer in the LLTO ceramic allowed us to adopt it as the solid-state electrolyte in a lithium–polysulfide cell. In the cell configuration, the LLTO solid-state electrolyte blocked the diffusion of the polysulfide catholyte and protected the lithium electrode, while the conventional solid sulfur cathode was replaced by a polysulfide catholyte absorbed into the cathode substrate[23,24] to create a wetted interface between the solid-state electrolyte and liquid-state catholyte for a close interface connection and strong reactivity.[20–22] Fig. 2d and e show the EIS analysis of the lithium/LLTO/polysulfide cell before and after cycling. The cycled cell maintained a similar resistance to that before cycling, which suggested that no polysulfide diffusion or sulfide re-deposition, which often causes high resistance in lithium–sulfur cells, had occurred. Normally, the high and middle frequency ranges reflect the effects of charge-transfer impedance and interface impedance, respectively.[7,32–35] The use of a polysulfide catholyte that was blocked by LLTO solid-state electrolyte might have enabled the relocation of the polysulfide by diffusion within the cathode to an electrochemically favorable position featuring a close connection with the carbon substrate.[30–32] The interface impedance also decreased after cycling, which suggested the existence of a smooth liquid/solid interface that was conducive to charge transfer.[7,33–37] Fig. 2f shows the cyclic voltammetry (CV) profile of the lithium–polysulfide cell in the voltage window of 1.5–3.0 V. The LLTO solid-state electrolyte enabled the resulting cell to undergo a standard lithium–sulfur electrochemical reaction. The profile, therefore, displayed two cathodic peaks and one anodic peak, which together represented the reversible solid–liquid–solid redox reaction of sulfur. The first cathodic peak, located at 2.10 V, can be attributed to the reduction of solid-state sulfur to liquid-state polysulfides ($S_8 \rightarrow Li_2S_{4-8}$). The second cathodic peak, located at 1.60 V, can be attributed to the reduction of polysulfides to sulfide ($Li_2S_{4-8} \rightarrow Li_2S_2/Li_2S$), a liquid-to-solid transition. The anodic peak, located at 2.80 V, can be attributed to the oxidation of lithium sulfide to lithium polysulfides and sulfur ($Li_2S_2/Li_2S \rightarrow Li_2S_8/S_8$).[4–6] During the repeated CV scanning, the CV curve showed no additional redox peaks, which confirmed the stable electrochemical reaction involving only the reversible discharging and charging reactions of sulfur. As a result, the material and electrochemical characteristics indicate the use of LLTO solid-state electrolyte as the solid-state electrolyte in the lithium–sulfur cell would offer stable electrochemical reactions. The passivated lithium electrode would have stable lithium-ion diffusion. The stabilized polysulfide cathode would contribute high and stable charge-storage capacity through the smooth electrolyte/catholyte interface.

Cell performance and characteristics

The lithium/lithium symmetric cell and the lithium–polysulfide cell with the LLTO solid-state electrolyte exhibited steady lithium-ion transfer and stable electrochemical reactions of the lithium–sulfur battery cathode. Fig. 3 summarizes the cell performance of the lithium–polysulfide cell with the use of the LLTO solid-state electrolyte. Fig. 3a and b show the cyclability analysis and discharge–charge voltage profiles of the lithium/LLTO/polysulfide cell cycled at a C/50 rate. The successful long-term cyclability confirmed the stability of the LLTO solid-state electrolyte and of the interface between the electrodes. Normally, lithium–sulfur cells with a solid-state electrolyte suffer from low electrochemical utilization and high interfacial resistance. However, the polysulfide catholyte possessed high reactivity and formed a smooth interface with the LLTO solid-state electrolyte. Thus, the cell with the LLTO solid-state electrolyte attained an excellent discharge capacity of 1429 mA h g^{-1}, corresponding to a high electrochemical utilization of sulfur over 85%. The cell maintained a high reversible capacity of 540 mA h g^{-1} and discharge–charge efficiency of 99% after 50 cycles. The corresponding discharge–charge voltage profiles confirmed the improved electrochemical reversibility and cycle stability (Fig. 3b). The use of a solid-state electrolyte inevitably resulted in a cell with high resistance. Nonetheless, the cell with the LLTO solid-state electrolyte maintained good cyclability, indicated by its stably completing the discharging reaction and showing two distinct discharge plateaus. The first discharge plateau occurred at 2.2–2.3 V, indicating the reduction of solid-state sulfur to liquid-state polysulfides (Li_2S_{4-8}), and the second occurred at 2.0–2.1 V, indicating the reduction of polysulfides to solid-state lithium sulfide. The reversible charging reaction from 2.25 V to 2.8 V completed the sulfide–polysulfide–sulfur conversion.[4–6] During cycling, the discharge and charge curves overlapped, which indicated good stability of the material chemistry and cell electrochemistry.

Fig. 3c shows that the cell cycled at a C/20 rate, which attained a high peak charge-storage capacity and maintained a high reversible capacity of 1178 mA h g^{-1} and 628 mA h g^{-1}, respectively, with a high electrochemical discharge–charge efficiency of 99%. As the current density increased, the cell continued to undergo a complete redox reaction with high electrochemical stability and reversibility (Fig. 3d). These experimental and analytical results suggest that the lithium–polysulfide cell with the LLTO solid-state electrolyte has good potential to serve as an advanced solid-state cell with high stability and safety. In the cell, the LLTO solid-state electrolyte restrained the rapid diffusion of liquid-state polysulfides, which would otherwise have harmed the cathode, and overcame the instability and unsafety issues faced by the lithium electrode. Moreover, although solid-state electrolytes have higher lithium-ion resistance than liquid electrolytes and therefore generate high interfacial resistance when connected to electrodes, the use of a polysulfide catholyte addressed this issue and enabled strong reactivity to boost the electrochemical utilization of the cell.[31,32]

Fig. 3e shows the rate capability of the LLTO solid-state electrolyte in the lithium–polysulfide cell with a wide range of cycling rates from C/50 to C/3. The cell attained high charge-storage capacities of 1,434, 768, 512, and 150 mA h g^{-1} at cycling rates of C/50, C/20, C/10, and C/3, respectively, and exhibited a stable discharge–charge efficiency approaching 99%. After completing the fast C/3-rate analysis, the cell was set back to the C/20 rate for an additional 50 cycles. When the

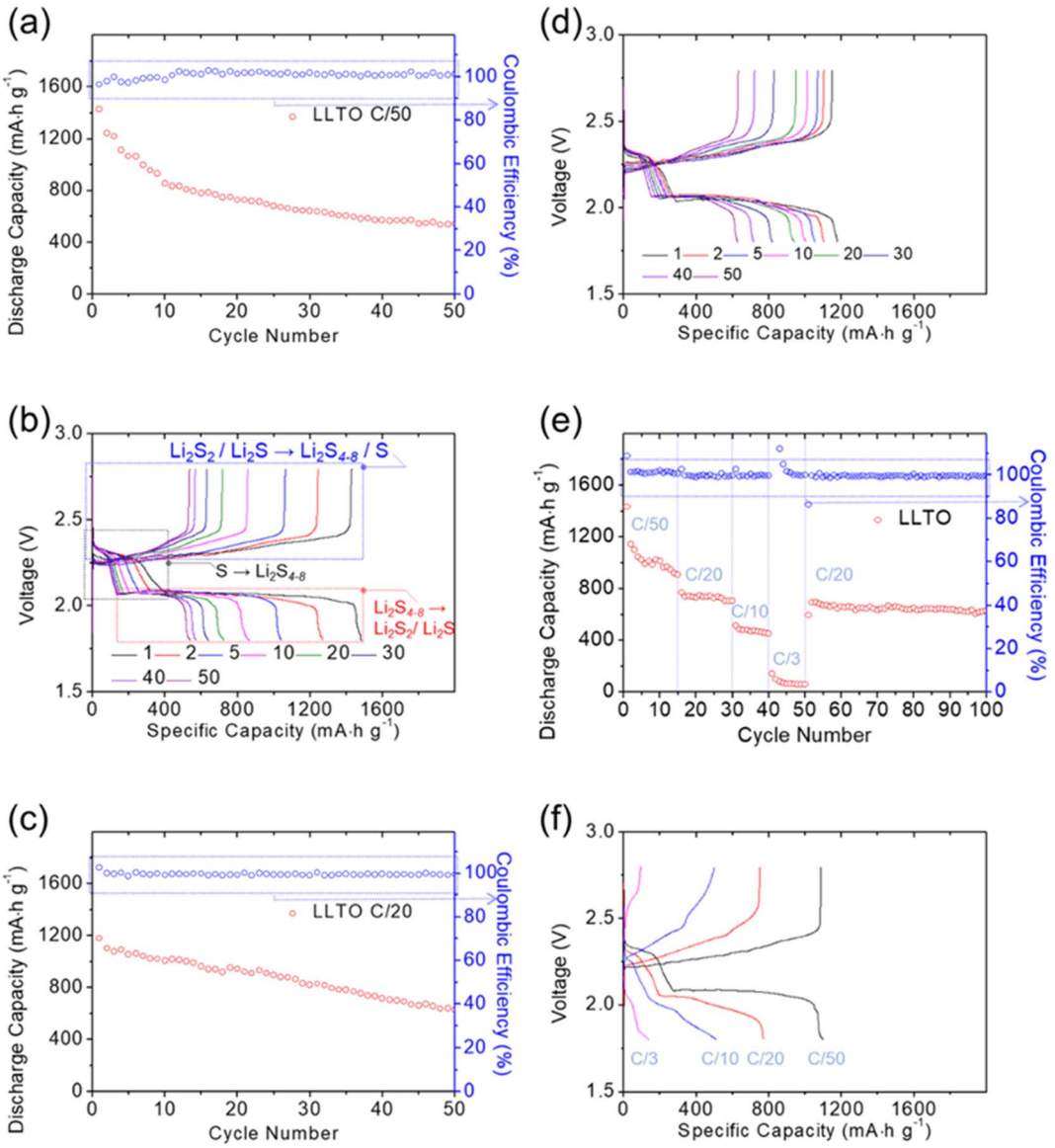

Fig. 3 Cell characteristics of LLTO solid-state electrolyte in a lithium–polysulfide cell: (a) cyclability at C/50, (b) discharge–charge curves of (a), (c) cyclability at C/20, (d) discharge–charge curves of (c), (e) rate performance, and (f) discharge–charge curves of (e).

cycling rate was set back to C/20, the cell displayed a high reversible capacity of 694 mA h g^{-1}, equivalent to a high retention rate of 99%, which indicated a negligible capacity loss during the rate-performance analysis. This confirmed the key function of the LLTO solid-state electrolyte in stabilizing the active polysulfide catholyte in the cathode for high electrochemical utilization. In the subsequent 50 cycles, the cell maintained a high reversible discharge capacity of 631 mA h g^{-1}, which demonstrated excellent cycle stability, characterized by a high capacity retention of 91% and a high discharge–charge efficiency value of 99.5%. Fig. 3f summarizes the complete discharge and charge voltage profiles at each cycling rate and confirms the high utilization and outstanding stability of the active material brought about by the LLTO solid-state electrolyte. In addition to the improved cyclability and rate performance, the cyclability and rate-performance measurements showed that the cells cycled at a C/50 rate had a high electrochemical utilization rate, while the cells cycled at a C/20 rate had a better capacity retention rate and cycle stability. This may be due to the C/50 rate, which allows a complete conversion reaction for high capacity; however, it also causes the formation of a large amount of insulating solid-state active materials. This results in a relatively rapid decrease in the high initial capacity achieved by the cells cycled at a low rate. Overall, Fig. 3 summarizes the lithium–sulfur cell characteristics and affirms the promising cyclability, stability, and rate capability of the LLTO solid-state electrolyte and the lithium/LLTO/polysulfide cell. This cell design exploits the advantages of the two most important cell components (*i.e.*, the lithium–sulfur battery cathode and the electrolyte) to address the drawbacks of each, which results in the high electrochemical utilization and stability of the cell.[8–10,37,38]

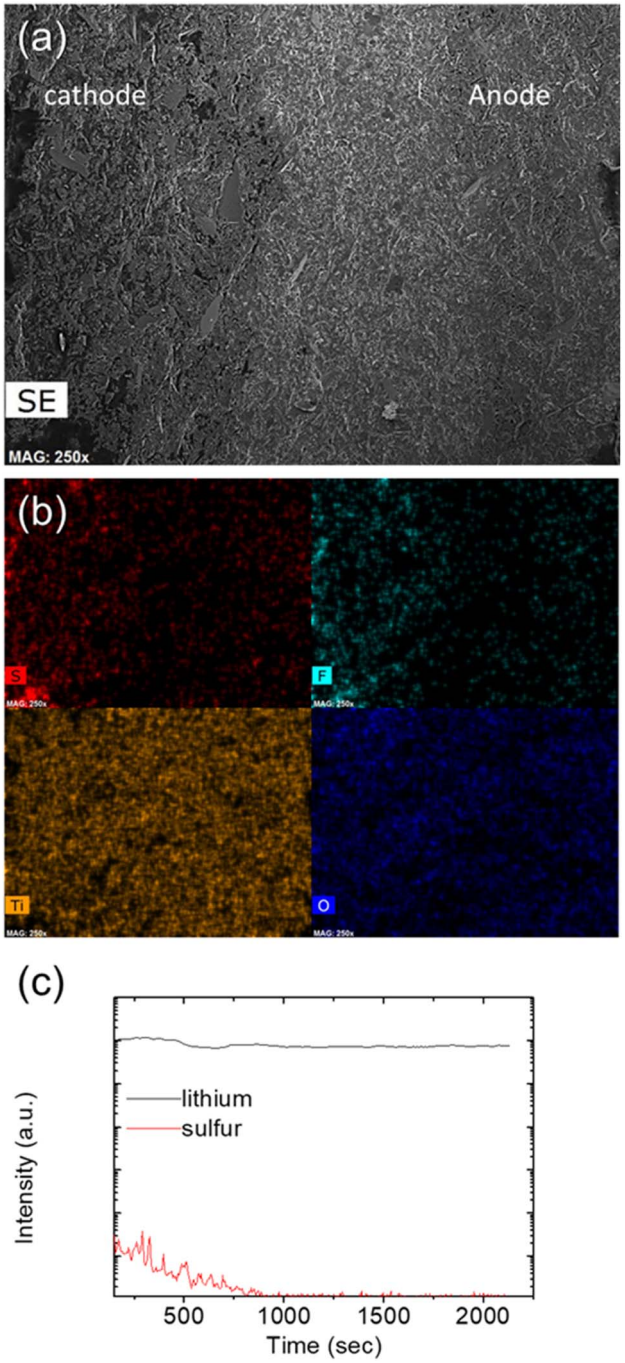

Fig. 4 Electrochemical/material analysis of the interface of the cycled LLTO solid-state electrolyte: (a) SEM cross-sectional microstructure, (b) energy-dispersive X-ray spectroscopy (EDS) elemental mapping results, and (c) secondary ion mass spectroscopy (SIMS) analysis of the cathode side.

In order to understand the concept proposed with a solid-state electrolyte and a polysulfide catholyte, the cycled LLTO solid-state electrolyte was retrieved from the cell for the elemental and corresponding morphological analyses (Fig. 4). In Fig. 4a and b, the cross-sectional SEM/EDS inspection of the cycled LLTO solid-state electrolyte from the cathode-facing side (left) to the anode-facing side (right) clearly revealed a change in the elemental sulfur signal, with a large amount of sulfur within the cathode region but only trace amounts in the LLTO and the anode-facing side, whereas there were no changes in the titanium and oxygen contents. These microstructural and elemental findings confirmed that the LLTO solid-state electrolyte retained sulfur within the cathode and that there was a smooth interface between the catholyte and the electrolyte. Moreover, Fig. 4c shows the results of secondary ion mass spectroscopy (SIMS) analysis of the cycled LLTO solid-state electrolyte. The intensity of the elemental sulfur signal decreased as the depth increased from the top cathode-facing surface to the cathode-facing side of the cycled LLTO solid-state electrolyte. The elemental lithium signal was much stronger than that of sulfur and maintained the same high intensity throughout the solid-state electrolyte. The precise intensity difference between elemental sulfur and lithium confirms the inhibition of polysulfides in the cathode region for high electrochemical stability and the formation of the smooth interface between polysulfide and LLTO solid-state electrolyte for the reduced interface impedance. Moreover, surface and cross-sectional microstructural and elemental analyses confirm that the LLTO provides the cell with two key benefits: high polysulfide retention and stable lithium-ion transfer.

As a short summary, the findings summarized in Fig. 4 confirm the strong polysulfide-diffusion blocking capability of the solid-state electrolyte and the formation of a polysulfide/LLTO interface, which contributed to the excellent polysulfide retention and low interface resistance. The LLTO solid-state electrolyte itself maintained good chemical stability and also assisted the stabilization of the electrodes. Taken together, these findings highlight the lithium/LLTO/polysulfide cell as a desirable cell configuration for the development of advanced lithium–sulfur cells with a solid-state electrolyte for a high electrochemical stability and safety.

Conclusions

In this study, we demonstrated the use of a polysulfide catholyte with strong reactivity and an LLTO solid-state electrolyte with high lithium-ion conductivity to fabricate an integrated lithium/LLTO/polysulfide cell configuration. The integrated optimization of these two post-lithium-ion technologies exploited the polysulfide catholyte's high redox-reactivity within a cell with a solid-state oxide electrolyte. The enhanced electrochemical utilization and stability contributed by these materials gave rise to a high charge-storage capacity of 1429 mA h g^{-1}, high rate performance at C/50 – C/3 rates, and high electrochemical efficiency above 99%. The LLTO solid-state electrolyte contributed to fast lithium-ion transfer and the restriction of polysulfide diffusion. The cross-sectional morphological analysis and elemental analysis confirmed that the LLTO solid-state electrolyte was sufficiently stable to block the diffusion of polysulfide out of the cathode and form a smooth liquid/solid interface for fast charge transfer. These results underline the promise of the configurational and material design of two post-lithium-ion technologies to equip energy-storage devices with improved energy density and safety.

Conflicts of interest

There are no conflicts to declare.

Acknowledgements

This work is supported by the Ministry of Education (MOE) in Taiwan under Yushan Young Scholar Program and the National Science and Technology Council (NSTC) in Taiwan under grants 112-2636-E-006-006 and 112-2923-E-006-004. This research was supported in part by Higher Education Sprout Project, Ministry of Education to the Headquarters of University Advancement at National Cheng Kung University. The authors gratefully acknowledge the use of XRD005100, EM003600, ESCA000200, and MS0000003300 under the grant 112-2731-M-006-001 belonging to the Core Facility Center of National Cheng Kung University.

Notes and references

1 Z. Piao, R. Gao, Y. Liu, G. Zhou and H.-M. Cheng, A Review on Regulating Li^+ Solvation Structures in Carbonate Electrolytes for Lithium Metal Batteries, *Adv. Mater.*, 2023, **35**, 2206009.

2 A. Manthiram and J. B. Goodenough, Layered Lithium Cobalt Oxide Cathodes, *Nat. Energy*, 2021, **6**, 323.

3 S. Feng, Z.-H. Fu, X. Chen and Q. Zhang, A Review on Theoretical Models for Lithium–Sulfur Battery Cathodes, *InfoMat*, 2022, **4**, e12304.

4 A. Deshmukh, M. Thripuranthaka, V. Chaturvedi, A. K. Das, V. Shelke and M. V. Shelke, A Review on Recent Advancements in Solid State Lithium–Sulfur Batteries: Fundamentals, Challenges, and Perspectives, *Prog. Energy*, 2022, **4**, 042001.

5 Q. Zhang, F. Li, J. Q. Huang and H. Li, Lithium–Sulfur Batteries: Co-existence of Challenges and Opportunities, *Adv. Funct. Mater.*, 2018, **28**, 1804589.

6 S.-H. Chung and A. Manthiram, Current Status and Future Prospects of Metal–Sulfur Batteries, *Adv. Mater.*, 2019, **31**, 1901125.

7 G. Zhang, Z. W. Zhang, H.-J. Peng, J.-Q. Huang and Q. Zhang, A Toolbox for Lithium–Sulfur Battery Research: Methods and Protocols, *Small Methods*, 2017, **1**, 1700134.

8 Y. Guo, S. Wu, Y.-B. He, F. Kang, L. Chen, H. Li and Q.-H. Yang, Solid-state Lithium Batteries: Safety and Prospects, *eScience*, 2022, **2**, 138–163.

9 J. Li, J. Qi, F. Jin, F. Zhang, L. Zheng, L. Tang, R. Huang, J. Xu, H. Chen, M. Liu, Y. Qiu, A. I. Cooper, Y. Shen and L. Chen, Room Temperature All-solid-state Lithium Batteries based on a Soluble Organic Cage Ionic Conductor, *Nat. Commun.*, 2022, **13**, 2031.

10 Y. Zheng, Y. Yao, J. Ou, M. Li, D. Luo, H. Dou, Z. Li, K. Amine, A. Yu and Z. Chen, A Review of Composite Solid-state Electrolytes for Lithium Batteries: Fundamentals, Key Materials and Advanced Structures, *Chem. Soc. Rev.*, 2020, **49**, 8790–8839.

11 C. Zheng, L. Li, K. Wang, C. Wang, J. Zhang, Y. Xia, H. Huang, C. Liang, Y. Gan, X. He, X. Tao and W. Zhang, Interfacial Reactions in Inorganic All-Solid-State Lithium Batteries, *Batteries Supercaps*, 2021, **4**, 8–38.

12 D. Lei, K. Shi, H. Ye, Z. Wan, Y. Wang, L. Shen, B. Li, Q.-H. Yang, F. Kang and Y. B. He, Progress and Perspective of Solid-State Lithium–Sulfur Batteries, *Adv. Funct. Mater.*, 2018, **28**, 1707570.

13 X. Huang, Z. Wang, R. Knibbe, B. Luo, S. A. Ahad, D. Sun and L. Wang, Cyclic Voltammetry in Lithium–Sulfur Batteries—Challenges and Opportunities, *Energy Technol.*, 2019, **7**, 1801001.

14 D. Lei, K. Shi, H. Ye, Z. Wan, Y. Wang, L. Shen, B. Li, Q.-H. Yang, F. Kang and Y.-B. He, Progress and Perspective of Solid-state Lithium–Sulfur Batteries, *Adv. Funct. Mater.*, 2018, **28**, 1707570.

15 X. Ji, K. T. Lee and L. F. Nazar, A Highly Ordered Nanostructured Carbon–Sulphur Cathode for Lithium–Sulphur Batteries, *Nat. Mater.*, 2019, **8**, 500–506.

16 S. Li, W. Zhang, J. Zheng, M. Lv, H. Song and L. Du, Inhibition of Polysulfide Shuttles in Li–S Batteries: Modified Separators and Solid-state Electrolytes, *Adv. Energy Mater.*, 2021, **11**, 2000779.

17 Q. Wang, Z. Wen, J. Jin, J. Guo, X. Huang, J. Yang and C. Chen, A Gel-ceramic Multi-layer Electrolyte for Long-life Lithium Sulfur Batteries, *Chem. Commun.*, 2016, **52**, 1637–1640.

18 Y. Fu, Y.-S. Su and A. Manthiram, Highly Reversible Lithium/Dissolved Polysulfide Batteries with Carbon Nanotube Electrodes, *Angew. Chem., Int. Ed.*, 2013, **52**, 6930–6935.

19 A. Manthiram and Y. Fu, *US Pat.*, 13793418, 2013.

20 Y. Inaguma, C. Liquan, M. Itoh, T. Nakamura, T. Uchida, H. Ikuta and M. Wakihara, High Ionic Conductivity in Lithium Lanthanum Titanate, *Solid State Commun.*, 1993, **86**, 689–693.

21 H. Kawai and J. Kuwano, Lithium Ion Conductivity of A-site Deficient Perovskite Solid Solution $La_{0.67-x}Li_{3x}TiO_3$, *J. Electrochem. Soc.*, 1994, **141**, L78.

22 A. G. Belous, G. N. Novitskaya, S. V. Polyanetskaya and Y. I. Gornikov, Investigation into Complex Oxide of the Composition $Ln_{2/3-x}Li_{3x}TiO_3$, *Izv. Akad. Nauk SSSR*, 1987, **23**, 470–472.

23 G. Li, S. Wang, Y. Zhang, M. Li, Z. Chen and J. Lu, Revisiting the Role of Polysulfides in Lithium–Sulfur Batteries, *Adv. Mater.*, 2018, **30**, 1705590.

24 Y. V. Mikhaylik and J. R. Akridge, Polysulfide Shuttle Study in the Li/S Battery System, *J. Electrochem. Soc.*, 2004, **151**, A1969.

25 B.-J. Lee, C. Zhao, J.-H. Yu, T.-H. Kang, H.-Y. Park, J. Kang, Y. Jung, X. Liu, T. Li, W. Xu, X.-B. Zuo, G.-L. Xu, K. Amine and J.-S. Yu, Development of High-energy Non-aqueous Lithium-Sulfur Batteries *via* Redox-active Interlayer Strategy, *Nat. Commun.*, 2022, **13**, 4629.

26 S. Nanda, A. Bhargav and A. Manthiram, Anode-free, Lean-electrolyte Lithium-Sulfur Batteries Enabled by Tellurium-stabilized Lithium Deposition, *Joule*, 2020, **4**, 1121–1135.

27 P. Borštnar, J. Žuntar, M. Spreitzer, G. Dražič and N. Daneu, Exaggerated grain growth and the development of coarse-

grained microstructures in lithium lanthanum titanate perovskite ceramics, *J. Eur. Ceram. Soc.*, 2023, **43**, 1017–1027.

28 Y.-C. Huang, H.-I. Hsiang and S.-H. Chung, Investigation and Design of High-Loading Sulfur Cathodes with a High-Performance Polysulfide Adsorbent for Electrochemically Stable Lithium–Sulfur Batteries, *ACS Sustainable Chem. Eng.*, 2022, **10**, 9254–9264.

29 G. Bieker, M. Winter and P. Bieker, Electrochemical *in situ* Investigations of SEI and Dendrite Formation on the Lithium Metal Anode, *Phys. Chem. Chem. Phys.*, 2015, **17**, 8670–8679.

30 Y. Ruan, Y. Lu, X. Huang, J. Su, C. Sun, J. Jin and Z. Wen, Acid Induced Conversion towards a Robust and Lithiophilic Interface for Li–$Li_7La_3Zr_2O_{12}$ Solid-State Batteries, *J. Mater. Chem. A*, 2019, **7**, 14565–14574.

31 Y.-J. Yen and S.-H. Chung, A Li_2S-Based Catholyte/Solid-State-Electrolyte Composite for Electrochemically Stable Lithium–Sulfur Batteries, *ACS Appl. Mater. Interfaces*, 2021, **13**, 58712–58722.

32 Y.-C. Huang, Y.-J. Yen and S.-H. Chung, Module-Designed Carbon-Coated Separators for High-Loading, High-Sulfur-Utilization Cathodes in Lithium–Sulfur Batteries, *Molecules*, 2022, **27**, 228.

33 S. D. Talian, G. Kapun, J. Moškon, R. Dominko and M. Gaberšček, Transmission Line Model Impedance Analysis of Lithium Sulfur Batteries: Influence of Lithium Sulfide Deposit Formed During Discharge and Self-Discharge, *J. Electrochem. Soc.*, 2022, **169**, 010529.

34 S. Waluś, C. Barchasz, R. Bouchet and F. Alloin, Electrochemical Impedance Spectroscopy Study of Lithium–Sulfur Batteries: Useful Technique to Reveal the Li/S Electrochemical Mechanism, *Electrochim. Acta*, 2020, **359**, 136944.

35 C.-C. Wu and S.-H. Chung, Material, Configuration, and Fabrication Designs for Lean-electrolyte Lithium–Sulfur Cell with a High-loading Sulfur Cathode, *J. Power Sources*, 2023, **566**, 232944.

36 Z. Han, R. Gao, Y. Jia, M. Zhang, Z. Lao, B. Chen, Q. Zhang, Q. Li, W. Lv and G. Zhou, Catalytic Effect in Li-S Batteries: From Band Theory to Practical Application, *Mater. Today*, 2022, **57**, 84–120.

37 G.-T. Yu and S.-H. Chung, Rational Design of a High-loading Polysulfide Cathode and a Thin-lithium Anode for Developing Lean-electrolyte Lithium–Sulfur Full Cells, *Small*, 2023, **20**, 2303490.

38 J. Yang, D. Lee, W. C. Yu, D. W. Kang, Y. Kim and J. W. Lee, Efficient Utilization of Lithium Polysulfides in CO_2-derived CNT Free-standing Electrode of Li-S Batteries, *Chem. Eng. J.*, 2023, **470**, 144337.